Surface Modification of Al_2O_3–$ZrO_2(Y_2O_3)$ Eutectic Oxides by Laser Melting: Processing and Wear Resistance

Francisco J. Ester and Rosa I. Merino*

Departamento de Física de la Materia Condensada, Instituto de Ciencia de Materiales de Aragón, C.S.I.C. Universidad de Zaragoza, 50009 Zaragoza, Spain

José Y. Pastor and Antonia Martin

Departamento de Ciencia de Materiales, Universidad Politécnica de Madrid, E. T. S. de Ingenieros de Caminos, 28040 Madrid, Spain

Javier Llorca*,†

Departamento de Ciencia de Materiales, Universidad Politécnica de Madrid & Instituto Madrileño de Estudios Avanzados en Materiales (IMDEA-Materiales), E. T. S. de Ingenieros de Caminos, 28040 Madrid, Spain.

Surface coatings of pseudo-binary Al_2O_3–$Zr_2O_3(Y_2O_3)$ eutectic oxides were produced by laser melting of the surface of conventionally sintered materials using a high-power diode laser. It was possible to obtain smooth, homogeneous, and crack-free coatings up to 50×7 mm^2 in area by carefully controlling the processing conditions (laser power, traveling speed of the specimen, and substrate temperature). The surface treatment was aimed at creating a dense, wear-resistant coating based on the eutectic microstructure generated upon solidification. The microstructure of the coating was formed by elongated colonies, and was similar to that found in rods grown by the laser-heated floating zone method at the same growth rates. The laser-melted coating presented much higher hardness and wear resistance than the sintered materials, and the optimum mechanical properties were measured in samples treated at 500 mm/h with a laser line power of 65–80 W/cm. These samples presented a hardness and wear rate of 19.7 ± 0.4 GPa and 3.8×10^{-6} mm^3/N m, respectively, while those of the conventionally sintered materials were 14.3 ± 0.2 GPa and 2.3×10^{-6} mm^3/N m.

I. Introduction

Melt-grown eutectic oxides have long been established as candidates for structural applications under extreme conditions due to the coupling of their ceramic nature with the inherent characteristics of the eutectic microstructure. The former includes high stiffness, hardness and melting point, and excellent oxidation resistance, whereas the latter provides a fine, homogeneous, and stable microstructure with a large surface area of strong interfaces free of glassy phases. Pioneer work carried out in the 1970s demonstrated the outstanding mechanical properties and the thermal and microstructural stability of directionally solidified eutectic ceramic oxides, as compared with that of conventional composites and monolithic ceramics.[1,2] Nevertheless, further improvements in properties were hindered by the limited thermal gradients in the solidification direction imposed by the Bridgman method ($< 10^2$ K/cm), which led to low growth rates and large interphase spacings (of the order of some microns).

New processing techniques developed since then (micro-pulling down, edge-defined film-fed growth, and, particularly, laser-heated floating zone methods) can reach thermal gradients up to 10^4 K/cm, and fast growth rates can be used in the coupled growth regime while interphase spacing is maintained below 1 μm.[3] This has led to renewed interest in these materials as new microstructures with novel properties can be achieved. In the realm of the mechanical properties, significant improvements in strength, creep, and oxidation resistance up to very high temperatures were reported in binary Al_2O_3–$Zr_2O_3(Y_2O_3)$ and Al_2O_3–$Y_3Al_5O_{12}$ as well as in ternary Al_2O_3–$Y_3Al_5O_{12}$–$Zr_2O_3(Y_2O_3)$ systems.[4–13] Bending strengths of 4.6 GPa, associated with high fracture toughness perpendicular to the rod axis, were recently reported in ceramic rods Al_2O_3–$Y_3Al_5O_{12}$–$Zr_2O_3(Y_2O_3)$ grown at very high rates (1200 mm/h) in a nitrogen atmosphere by the laser-heated floating zone method.[14] These properties are induced by the nonconventional microstructure obtained under these conditions, which is formed by bundles of single-crystal c-oriented Al_2O_3 and $Y_3Al_5O_{12}$ whiskers of ≈100 nm width with smaller YSZ whiskers between them. In the area of wear resistance, near-eutectic Al_2O_3–$Zr_2O_3(Y_2O_3)$ rods grown by the laser-heated floating zone method were subjected to reciprocating sliding friction experiments against B_4C and showed an acceptable behavior for wear-resistant applications in the temperature range 296–1073 K.[15]

Large longitudinal thermal gradients upon solidification also induce large thermal gradients in the radial direction that increase with the axial gradient and the specimen thickness or radius. This leads to the development of large thermal stresses in the radial direction and to fracture should the eutectic oxide sample be thicker than a few mm.[3] This is an important limitation for the practical application of eutectic oxides that can be overcome through the laser-assisted melting of eutectic oxide plates, particularly in improving surface-controlled properties like wear resistance. The feasibility of this technique has been demonstrated in previous investigations[16–18] but it was limited to small areas (in the range of a few mm^2) due to a tendency to crack and trap bubbles within the advancing solidification front. Other researchers have also recently investigated the possibility of crack-free surface densification of Al_2O_3-based porous refractories by laser surface treatment.[19] Nevertheless, cracking and bubble formation problems have been largely overcome in this investigation and this achievement is an important step forward to manufacture large surfaces of melted refractory ceramic

oxides without compromising the mechanical integrity of the ceramic piece. This procedure was applied to Al_2O_3–$Zr_2O_3(Y_2O_3)$ eutectic oxides to create surface coatings with higher density and wear resistance, which are expected to show excellent erosion and oxidation resistance as well. Therefore, important applications can be envisaged as protective tiles for high-temperature applications in aggressive environments in aerospace and energy generation sectors. In this work, large surfaces (50×7 mm^2) of Al_2O_3–$Zr_2O_3(Y_2O_3)$ eutectic oxide dense plates were recrystallized using a high-power diode laser at scanning rates in the range 20–3000 mm/h. The thickness of the melted layer was approximately 400 μm and the wear resistance of melted samples were measured in an oscillating sliding friction machine against MgO partially stabilized ZrO_2 spheres. The results of the wear tests, together with the analysis of the fracture micromechanisms, provided new insights into the effect of the microstructure in the wear properties of these eutectic oxides.

II. Processing and Experimental Techniques

(1) Processing

Ceramic plates with densities of around 95% were prepared by slip casting of aqueous suspensions with a solid content of 60 wt%. The powder mixture was prepared with 57.9 wt% of Al_2O_3 (HPA-0.5 C10214, 99.99% from Sasol North America, Ceralox Division, Tucson, AZ), 41.13 wt% of tetragonal ZrO_2 stabilized with 3 mol% of Y_2O_3 (from Tosho, Japan, 99.9%, $d_{50} = 0.25$ μm), and 0.92 wt% of Mn_2O_3 (99% Aldrich). They were thoroughly mixed, dispersed, and suspended in water using Duramax D-3005 (Rohm and Haas Company, Philadelphia, PA) as dispersant. The suspension was continuously mixed for at least 4 hours before casting. The green compacts were dried overnight and presintered at 1000°C for 3 hours, cut almost to the final size, and sintered at 1500°C for 2 hours. The pieces were then carefully machined into rectangular bars with typical dimensions $25 \times 7 \times 5$ mm^3 (and longer) before laser surface processing.

The samples were placed on a hot plate that could be heated up to 1100°C and moved along one direction at a constant speed. The sample movement was parallel to the longest dimension of the bar and traveling speeds in the range 20–1500 mm/h were used. The sample and the hot plate were placed within a chamber, and the experiments carried out at atmospheric pressure in laboratory air, although a protecting gas (N_2) atmosphere could be pumped into the chamber whenever required to prevent the formation of O_2 bubbles. The surfaces of the samples were melted with a focused diode laser line (DL-X50, $l = 940 +- 10$ nm, from Rofin-Sinar Laser GmbH, Hamburg, Germany) of dimensions 1×10 mm^2, the longest dimension of the beam perpendicular to the sample movement.

The temperature of the hot plate was set to 980°C, as measured with a type-K thermocouple. Selected experiments were monitored using a CCD photographic camera (Nikon-D100, Nikon Corporation, Natori, Japan) equipped with a red interference filter before the objective (monochromatic light photograph) to measure the thermal gradient at the solid–liquid interface. The images obtained with the camera were processed numerically and the light intensity was converted to true temperature using the calibration procedure described elsewhere.[20] In addition, the depth of the melted pool was measured after processing.

(2) Microstructural Characterization

The surface roughness and planarity of the samples were measured with an optical confocal profilometer (Dual Sensofar PLμ 2300, Sensofar-Tech, S.L., Terrasa, Spain) with a maximum lateral resolution of 0.3 μm. In addition, the sample surfaces were observed in a scanning electron microscope (Model 6400, Jeol, Tokyo, Japan).

(3) Mechanical Characterization

The Vickers hardness of the melted surfaces was measured with a microhardness tester (Model MVK-E II, Akashi, Japan). The specimens were slightly polished to reduce the scatter and loaded with 4.9 N for 15 s. The length of the cracks emanating from the indentation corners was measured in the optical microscope, and the fracture toughness K_C was computed from the equation proposed by Anstis *et al.*[21] for median radial cracks from the indentation load (4.9 N), the hardness, and the elastic modulus (310 GPa for Al_2O_3–$ZrO2(Y_2O_3)$ eutectics[3]).

Wear tests were carried out in an oscillating sliding friction machine (Model 77, Cameron-Plint, Wokingham, U.K.) by rubbing 3.5 mol% MgO partially stabilized ZrO_2 spheres (Morgan Matroc Technical Ceramics, Stourport, U.K.) of 5 mm diameter against the surface of the laser-treated plates. The hardness and toughness of the ceramic spheres were, respectively, 11 GPa and 8.5 MPa$\sqrt{}$m. The spheres were gripped to avoid rolling during the test and the spheres and the plate surface were cleaned in ultrasound in acetone before testing. All the tests were carried out in a laboratory atmosphere (room temperature 22 ± 3°C and relative humidity 33 ± 5%) under a normal force of 50 N. The tangential friction force was monitored continuously with a piezoelectric transducer attached to the holder table that supported the plate. The amplitude of the sphere oscillating movement was 15 mm and the frequency was 10 Hz. Specimens were not lubricated and the wear loss was determined by the difference in weight before and after testing, which was measured with an electronic balance (AG 245 Mettler-Toledo, Küsnatht, Switzerland) with a resolution of 0.01 mg. The weight loss was transformed into volume loss by measuring the density through the Archimedes method in ethanol. The sliding distance at the end of the test was 540 m. Additional details about the experimental set up can be found in Martin and colleagues.[22,23]

Once tested, the samples were cut through the middle along the traveling direction, initially polished using a diamond of 30 μm grain size as an abrasive, and afterwards with a diamond slurry (up to 1 μm). The polished surfaces were coated with a thin layer of Au and the dominant fracture mechanisms were determined from the observation of the transverse sections in the scanning electron microscope. Polished cross sections of the as-processed samples were also examined in the scanning electron microscope before testing with the aim of measuring the microstructural features (colony diameter, interlamellar spacing, and intercolony thickness). This information is important to relate the microstructure to the mechanical properties.

III. Microstructure

The laser-melted ceramics presented a flat and shiny surface, as shown in Fig. 1 for a sample treated at a traveling speed of 500 mm/h. The sample borders are rounded due to the shape of the melted surface produced during processing. One vertical shadow, approximately at 12 mm from the right end, can be seen on the surface. Its origin will be explained later. Regardless of this feature, the microscopic roughness of these surfaces was very small. Figures 2(a) and (b) show the same area of the bare surface observed in the scanning electron microscope with backscattered electrons and in the topographic mode, respectively. They suggest a very smooth surface with some relief, whose amplitude is of the order of the underlying microstructural dimensions. Slightly deeper grooves were found at the boundary between colonies (marked with an arrow in both images). These observations were corroborated by means of optical profilometry. Figure 3(a) shows a scan of an area of 140×105 μm of a

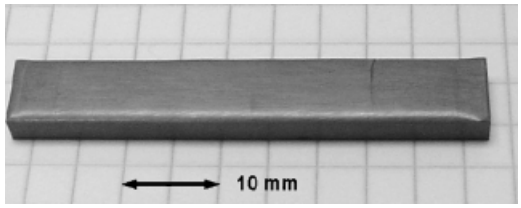

Fig. 1. Photograph of an Al_2O_3–ZrO_2 (Y_2O_3) prismatic specimen whose surface was laser melted at a traveling speed of 500 mm/h.

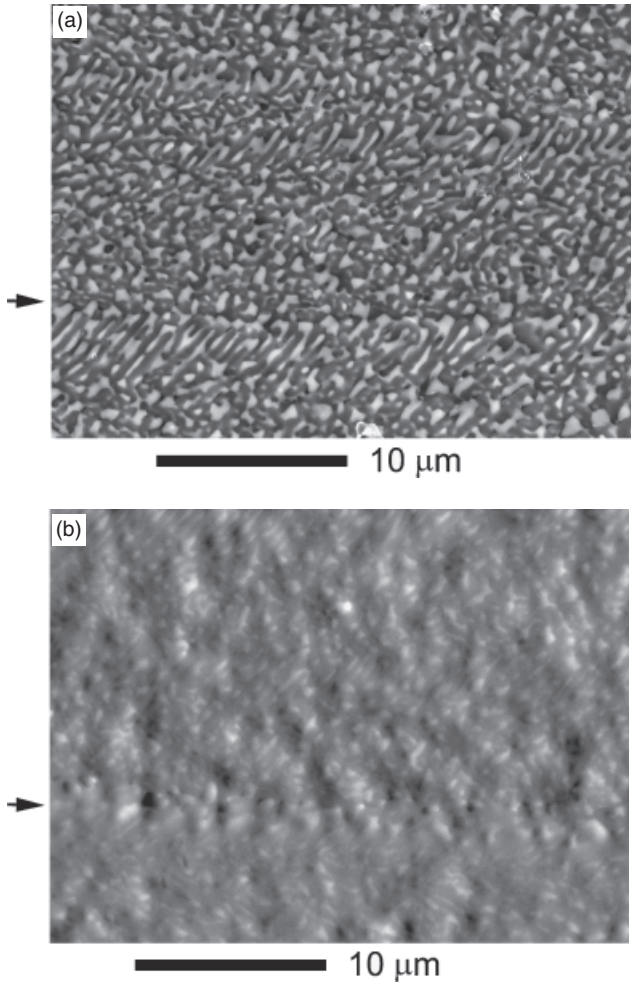

Fig. 2. Scanning electron micrographs of the laser-melted surface (traveling speed of 500 mm/h). (a) Backscattered electron image: Al_2O_3 appears black and ZrO_2 appears white; (b) Topographic mode.

sample processed at 1500 mm/h. The average roughness (R_a), measured without filtering, associated with this area was 0.14 μm. The maximum height of the profile was 1.1 μm. The valleys and peaks reproduced the colony microstructure obtained by laser melting, which is detailed below. Banding was found at larger length scales (1 × 1 mm), as shown in Fig. 3(b). This figure shows the topography of the surface obtained with the optical confocal microscope. The upper half is shown in topographic mode, which gives a stronger contrast. The lower half of the image is presented as a contour plot, with grayscale levels indicating height (left scale in the Fig. 3(b)). The processing direction was parallel to the longer dimension of the figure. The elongated features, running horizontally, show the solidification direction of the colonies. In addition, small bands perpendicular to the traveling direction developed on average every 170 μm, with an amplitude of 2 μm. They were probably associated with local, high-frequency and low-intensity instabilities of the processing equipment, melt drop, and/or solidification instabilities. Less frequent instabilities gave rise to the large wavelength wavy profile with an amplitude around 5.5 μm in this particular image (see the contour plot scale in Fig. 3(b)). It is very likely that they were due to laser power fluctuations or mechanical perturbation of the processing equipment. One perturbation of this type (with an even longer amplitude of ≈40 μm) caused the shadow line in Fig. 1, which can be seen with the naked eye. Once these long wavelength undulations were filtered, the average roughness was 0.3 μm, slightly higher than the one measured in Fig. 3(a).

The depth of the melted layer at the center of the specimens increased almost linearly with laser power (Fig. 4). Differences among specimens with different widths (4–7 mm) were minimal.

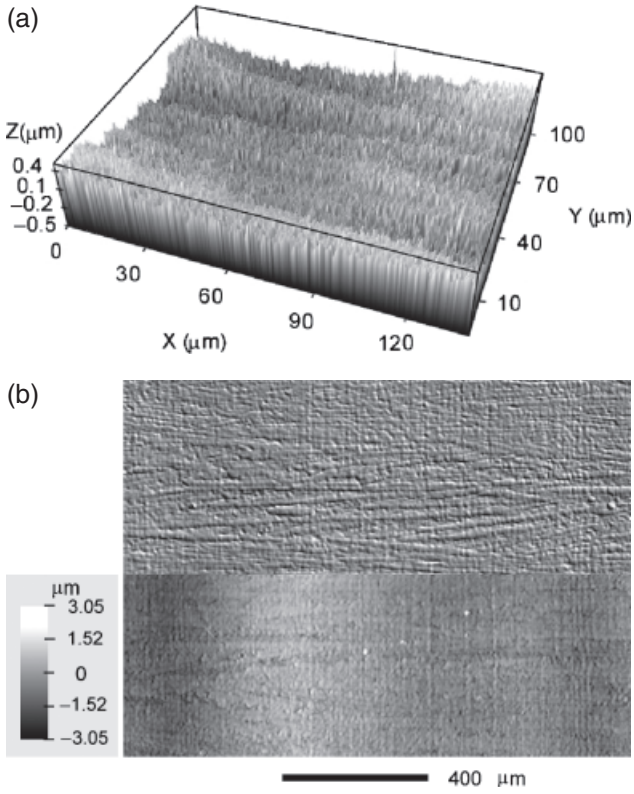

Fig. 3. Topography of the laser-melted surface processed at 1500 mm/h. (a) Topography of an area of 140 × 105 μm. (b) Topography of an area of 1.4 × 1.05 mm^2: the upper half image is shown in the topographic mode; the lower part shows a contour plot image, in which the height is given by the gray scale on the left. The laser scanning direction runs parallel to the longer dimension of both images.

The data plotted in Fig. 4 correspond to experiments performed sequentially, on samples of the same size, to avoid dispersion caused by uncontrolled differences in the hot plate, temperature, or laser aging. Under these conditions, the standard deviation of each point was below 10 μm. Extrapolation of the results in

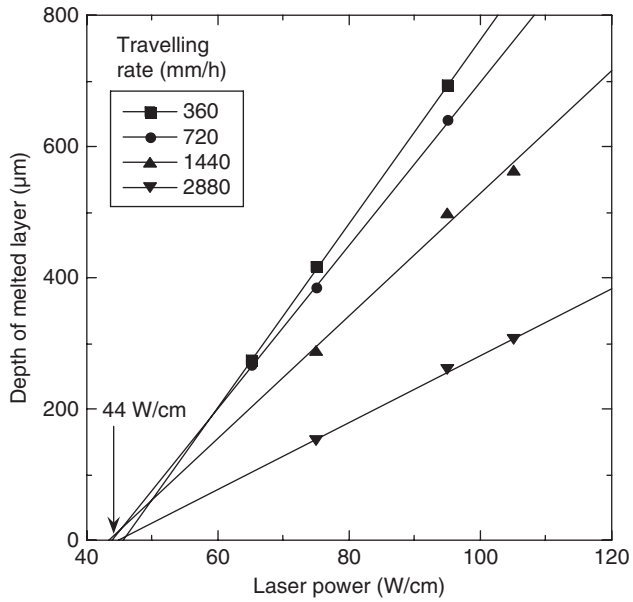

Fig. 4. Depth of the melted zone at the center of the sample as a function of the laser power output at different traveling speeds. The specimens were preheated at 980°C. The laser power is given as power per unit length because it was distributed homogeneously along a line of 1 cm. The line width was ≈1 mm with an approximate Gaussian power distribution.

Fig. 4 led to an estimation of 44 W/cm for the minimum power to initiate melting when the width of the laser beam was 1 mm and the specimens were preheated at 980°C. This threshold power was practically independent of the traveling speed. These experimental results were used to select the optimum processing conditions to fulfill two objectives. The first one was to create at the specimen surface a microstructure whose features were equivalent to those obtained by the laser-heated floating method in rods, which have shown excellent flexural strength and creep resistance.[5,12] These microstructures were generated when the growth rate was in the range 100 and 1500 mm/h; these traveling speeds were used in the surface melting experiments. Secondly, it was necessary to create homogeneous layers free from defects, and this required melt depths thicker than 100 μm to ensure the homogeneity of the molten layer. Consequently, the laser power was adjusted to create a melted layer between 250 and 500 μm in thickness for each traveling speed. This thickness is large enough to guarantee that the wear properties of the specimen are controlled by the behavior of the laser melted region and, in addition, is small enough to prevent bubble trapping or cracking of the layer during processing.

In fact, bubbles began to appear at traveling speeds above 1000 mm/h, even when the laser beam was fully focused on the surface to reach the maximum temperature and the minimum viscosity, and the sintered ceramic specimen was fully dense. These bubbles appear as a result of the exolution of oxygen upon melt cooling.[24] The number and size of the bubbles decreased significantly when laser melting was carried out under a nitrogen atmosphere, to prevent the dissolution of oxygen into the melt. Nevertheless, a few remaining bubbles were always formed at the highest traveling speeds. They were often located at the interface between the sintered ceramic and the laser-melted layer (as was also observed by Triantafyllidis *et al.*[25]), and did not influence either the wear behavior or the surface roughness.

The solidification process generates large thermal gradients in the material at the solid–liquid interface, as well as in the solidifying layer and the surrounding solid material. This may result in catastrophic failure or surface cracking under unfavorable conditions.[26] Given that determination and control of the thermal stresses is a critical aspect to optimize the laser treatment, the temperature field was measured on the surface by optical means, as indicated in the previous section. It was found that the thermal gradient at the surface around the solidifying interface decreased from 700°C/mm at a traveling speed of 360 mm/h to 420°C/mm at 1360 mm/h. The reduction in the thermal gradient with traveling speed was due to the competition between the traveling rate (which shifts the point at which the heat source is located) and the cooling of the solid–liquid interface by thermal conduction to the solidified layer and the adjacent ceramic material. These thermal gradients are similar to those found in bars grown by the laser-heated floating-zone method using a CO_2 laser as a power source.[27] Nevertheless, the diameter of the rods grown by the laser-heated floating zone method is limited to a few mm while surface melting of larger surface widths is possible without cracking if the ceramic substrate is preheated at around 1000°C. At this temperature, plastic deformation can take place, relieving the thermal residual stresses.[11]

As the thermal gradients at the solid–liquid interface were the same in the rods processed by the laser-heated floating zone method and during surface remelting, the same growth regimes were expected in both situations,[27] and this was indeed the case. The microstructure of the melted layers processed at traveling speeds above 100 mm/h showed the presence of eutectic elongated colonies (or cells) surrounded by regions of coarser microstructure (Fig. 5). This cellular microstructure showed a somewhat different phase arrangement inside the cells depending on the traveling speed: disordered phase arrangement at 100 mm/h (Fig. 5(a)), strongly faceted colonies at 200 mm/h (Fig. 5(b)), and lamellar ordering above 1000 mm/h (Fig. 5(c)).

The size of the microstructural features of the uppermost layer adjacent to the surface decreased as the traveling rate

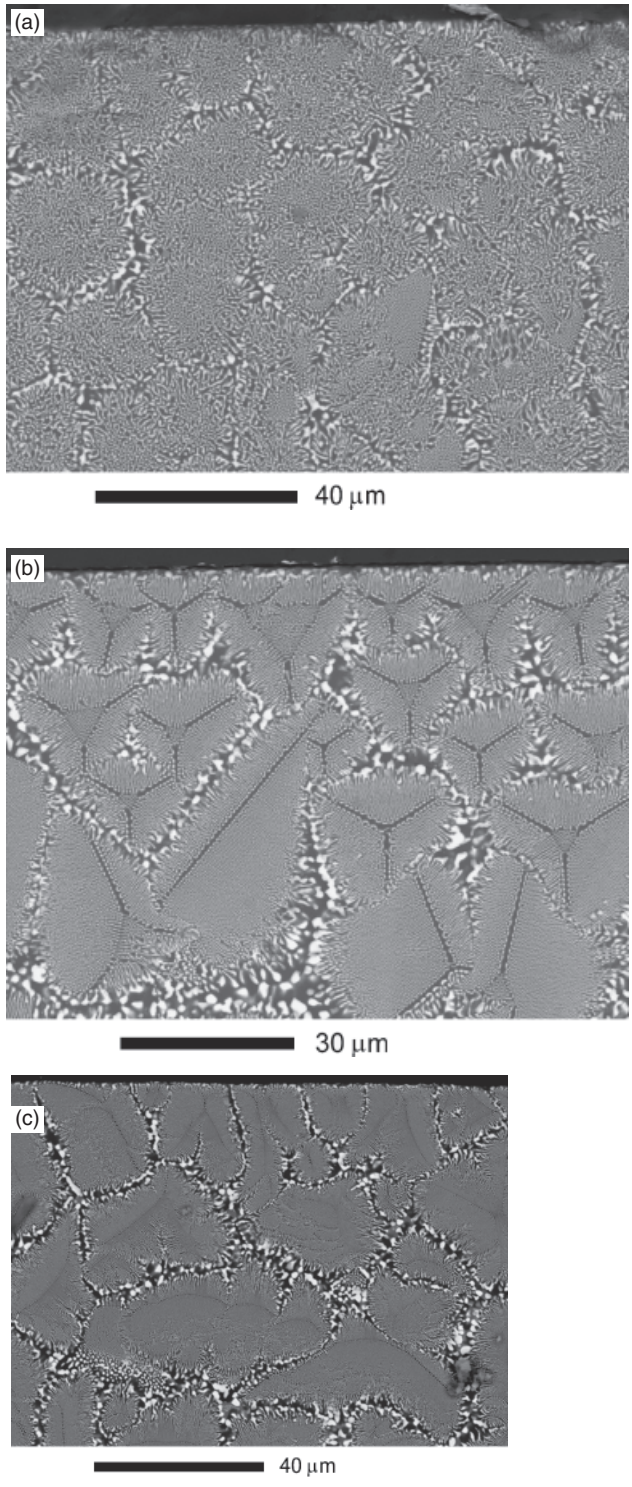

Fig. 5. Scanning electron micrographs of the transverse cross section near the surface of laser-melted specimens. The traveling speeds were (a) 100 mm/h; (b) 200 mm/h; and (c) 500 mm/h.

increased (Fig. 5). Only this area, up to a maximum depth of 20 μm, was removed in the wear experiments shown in the next section. The intercolony regions were made up of a coarser two-phase microstructure. The colony diameter and the thickness of the intercolony regions were estimated from the micrographs of the crosssections. The interphase spacing (average distance between equal phases) within the colonies was determined from

Table I. Microstructural Features of Al_2O_3–$ZrO_2(Y_2O_3)$ Eutectic Oxides at the Surface as a Function of the Traveling Speed

Traveling speed (mm/h)	Interlamellar spacing (μm)	Colony diameter (μm)	Intercolony thickness (μm)
100	0.75	22	3.0
200	0.4	18	3.5
500	0.3	17	2.5
1000	0.17	12	2.2
1500	0.17	13	1.2

Fourier Transform analysis. The dimensions of these relevant microstructural parameters are summarized in Table I as a function of the traveling speed, and they always decreased as the traveling speed increased. Interphase spacing and average colony size at the surface tended to saturate at 1000 mm/h, while the intercolony thickness diminished continuously with the traveling speed. Defects (in the form of voids or cracks) were concentrated in these intercolony regions, particularly at higher solidification rates.

IV. Mechanical Properties

(1) Hardness and Fracture Toughness

The average value and the standard deviation of the hardness (corresponding to at least ten indentations in each sample) are plotted in Fig. 6 for the sintered and laser-melted plates. It was clear that laser melting increased the hardness by about 30% and the hardness of the samples treated between 100 and 500 mm/h was in the range (18–20 GPa) reported in the literature for directionally solidified Al_2O_3–$Zr_2O_3(Y_2O_3)$ eutectic oxides.[5,12,28] Higher processing speeds led to a reduction in hardness, which can be attributed to the trapping of residual porosity at the colony boundaries at higher growth rates.

The fracture toughness of the laser-melted surfaces was in the range 6–7 $MPa\sqrt{m}$. It was not possible to discriminate any effect of the processing speed, given that the experimental values showed a large dispersion, mainly due to the irregular nature of the crack and the difficulties in determining the crack length. These problems arose because the surfaces were only very lightly polished before indentation to test the actual microstructure created after laser melting.

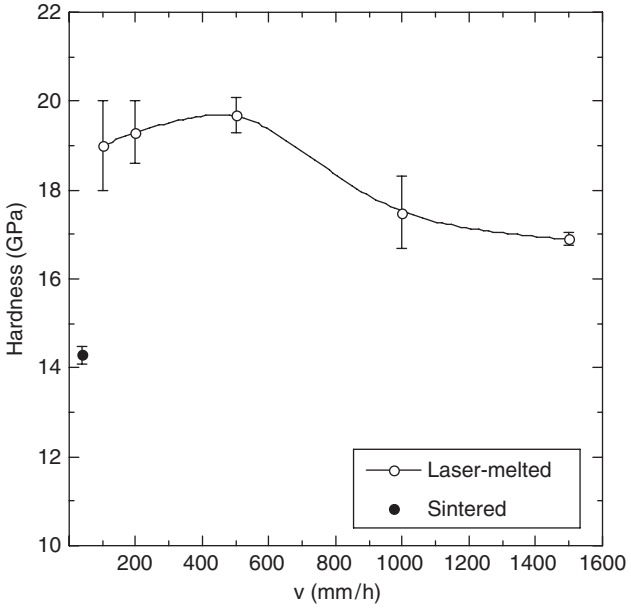

Fig. 6. Hardness of the sintered and laser-melted Al_2O_3–$ZrO_2(Y_2O_3)$ eutectic oxides. The error bars stand for the standard deviation of at least 10 indentations.

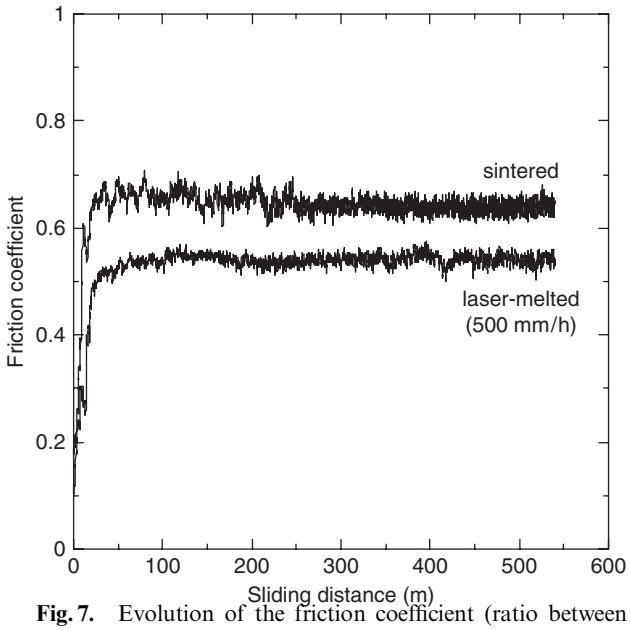

Fig. 7. Evolution of the friction coefficient (ratio between tangential and normal force) as a function of the sliding distance for the sintered sample and the laser-melted one at 500 mm/h.

(2) Wear Resistance

It was possible to perform the wear tests on the as-processed plates due to the quality of the surfaces as evinced by their flatness and minimum surface roughness. Tests were performed along the processing direction. A minimum of four wear tests were carried out for each sample. Representative results of the evolution of the friction coefficient (ratio between tangential and normal forces) are plotted in Fig. 7 for the sintered samples and those laser melted at 500 mm/h. Those remaining are not plotted as they present similar trends, characterized by an initial increase up to a maximum, followed by a gradual reduction until a constant value. The initial transitory period can be attributed to the original surface roughness of the bodies in contact and disappeared rapidly as the wear process modified the surfaces in contact. The steady-state situation was reached after $\approx$100 m, $<$20% of the total sliding distance. The evolution of the steady-state friction coefficient is plotted in Fig. 8(a) as a function of the processing rate. The friction coefficients were high in all cases, as expected from unlubricated wear tests, but the scatter was limited, and the differences found in Fig. 8(a) could be considered representative of the behavior of the different materials. In particular, the friction coefficient of the tests on laser-melted surfaces was always lower than the one measured in sintered plates; also the, minimum friction coefficient was found in laser-melted materials processed between 200 and 500 mm/h.

The specific wear resistance of each material (defined as the wear volume at the end of the test divided by the sliding distance and the normal force) is plotted in Fig. 8(b). It is important to note that the absolute magnitude of the wear resistances in Fig. 8(b) depends on the nature of the rubbing surfaces (Mg-PSZ spheres against Al_2O_3–$Zr_2O_3(Y_2O_3)$ eutectic oxides) and the experimental setup (oscillating friction of a sphere on a plate without lubrication and rolling), and it is difficult to make direct comparisons with other tests. Nevertheless, the specific wear resistances of the laser-melted surfaces were similar to those reported by Miyoshi *et al.*[15] for eutectic and near-eutectic Al_2O_3–$Zr_2O_3(Y_2O_3)$ rods rubbed against B_4C plates without lubrication. In addition, they were equivalent to those measured with the same experimental setup and testing conditions (load, sliding speed, counterbody shape and material, etc.) in Al_2O_3/SiC[23] and Al_2O_3/ZrO_2[29] nanocomposites with enhanced wear resistance.

The specific wear rate was minimal for the plates processed at 500 mm/h, which coincided with the maximum hardness and minimum friction coefficient. The wear resistance of plates

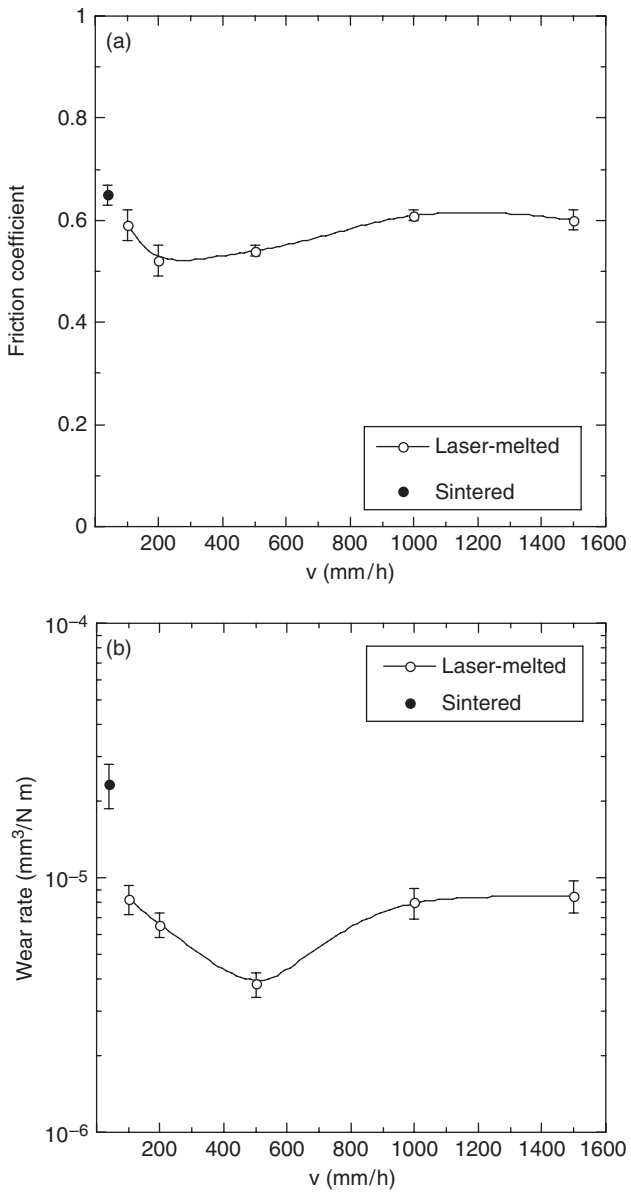

Fig. 8. (a) Average steady-state friction coefficient as a function of the processing speed of the laser-melted surfaces. (b) *Idem* for the specific wear resistance. The error bars stand for the standard deviation of, at least, four tests. The behavior of the sintered eutectic oxide is also plotted for comparison.

processed at higher or lower speeds decreased and was accompanied by a slight reduction in hardness and an increase in the friction coefficient. The wear resistance of the laser-melted surfaces was always superior to that of the sintered material. The maximum differences were found in the bars processed at 500 mm/h, whose wear rate was 3.8×10^{-6} mm^3/N m, while that of the conventionally sintered material was 2.3×10^{-6} mm^3/N m. It should be noted that the wear rates reported here for the sintered material were equivalent to those found in sintered zirconia-toughened alumina composites also measured with the same experimental setup and testing conditions.[30]

The physical mechanisms responsible for the differences in wear resistance among the laser-melted surfaces and the sintered material can be ascertained from the analyses of the deformation and fracture processes. Scanning electron micrographs of the worn surface and of a crosssection perpendicular to the worn surface are shown in Figs. 9(a) and (b), respectively, for the laser-melted plate with the highest wear resistance (500 mm/h). The worn surface was smooth and there were no traces of subsurface damage in the crosssection, indicating that wear took

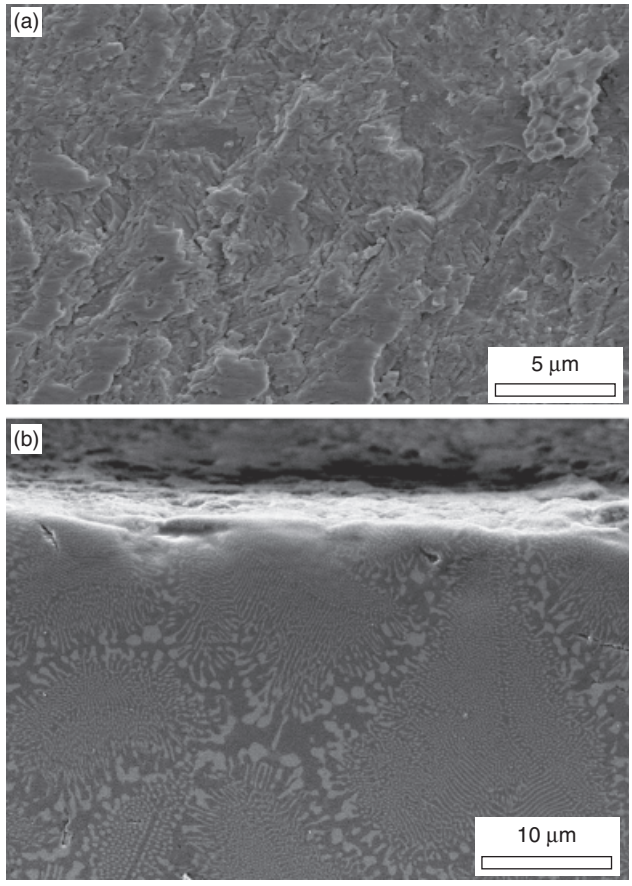

Fig. 9. Wear mechanisms in the laser-melted surfaces processed at 500 mm/h, which showed the highest wear resistance. (a) Scanning electron micrograph of the worn surface. (b) Scanning electron micrograph of a cross section perpendicular to the worn surface.

place by an abrasive mechanism in which thin surface layers of material were plastically deformed until fracture as a result of large contact stresses.[‡] This process continued progressively during the test, leading to a reduced wear rate, typical of the mild wear regime.

The worn surface and the crosssection corresponding to the laser-melted surfaces processed at 1500 mm/h are shown in Fig. 10(a) and (b), respectively. They revealed that, in addition to abrasion, debris formation took place by the development of cracks at the intercolony areas (Fig, 10(b)). While the intercolony regions in the samples processed at a low speed (< 500 mm/h) were dense (Fig. 9(b)), this was not the case in the samples processed at a high speed, in which many pores were found (Fig. 10(b)). The defects at intercolony regions promoted the nucleation of cracks under the action of the contact stresses; wear progressed by the successive pull-out of micrometer-sized fragments as the subsurface cracks propagated. This process led to rougher contact surfaces and was also responsible for the higher friction coefficient and wear rates.

Laser-melted surfaces processed at a low speed (≤ 500 mm/h) did not show evidence of pores at the intercolony areas (Fig. 9(a)) or subsurface cracks, and wear proceeded by the abrasive mechanism described above. The origin of the reduction in wear resistance with the processing speed was not particularly clear although it could be associated with the slight differences in hardness and also with the coarser microstructure (lamella spacing, colony diameter, and intercolony width).

All such observations highlight that the optimum microstructure from the viewpoint of wear resistance should be made up of a fine dispersion of tetragonal ZrO_2 platelets or rods dispersed

[‡]The maximum value of the contact stress at the beginning of the tests was approximately 0.7 GPa, as it can be easily determined from the elastic moduli of the sphere and the plate, the sphere radius, and the normal force using the expression deduced by Hertz.[15]

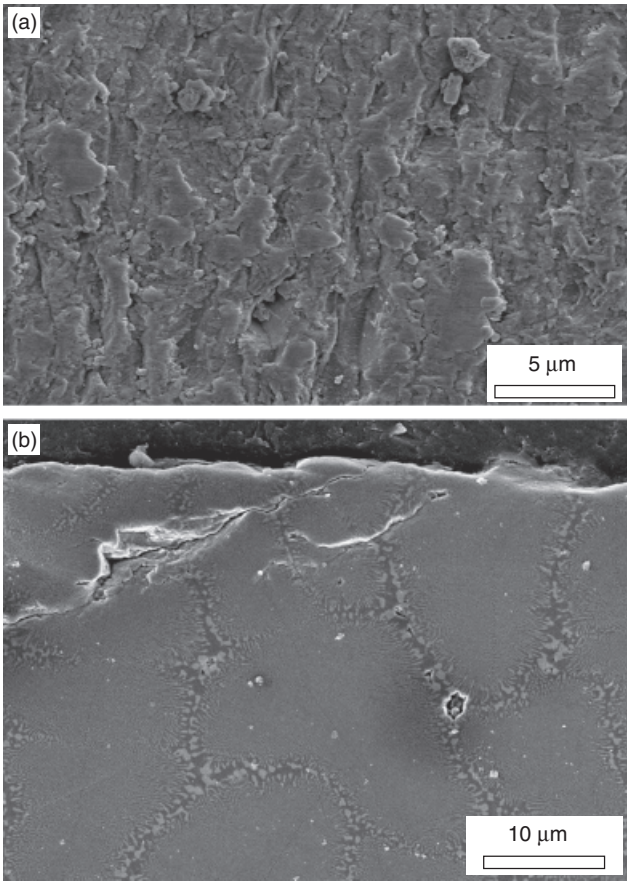

Fig. 10. Wear mechanisms in the laser-melted surfaces processed at 1500 mm/h. (a) Scanning electron micrograph of the worn surface. (b) Scanning electron micrograph of a cross section perpendicular to the worn surface. Note the porosity at the intercolony regions.

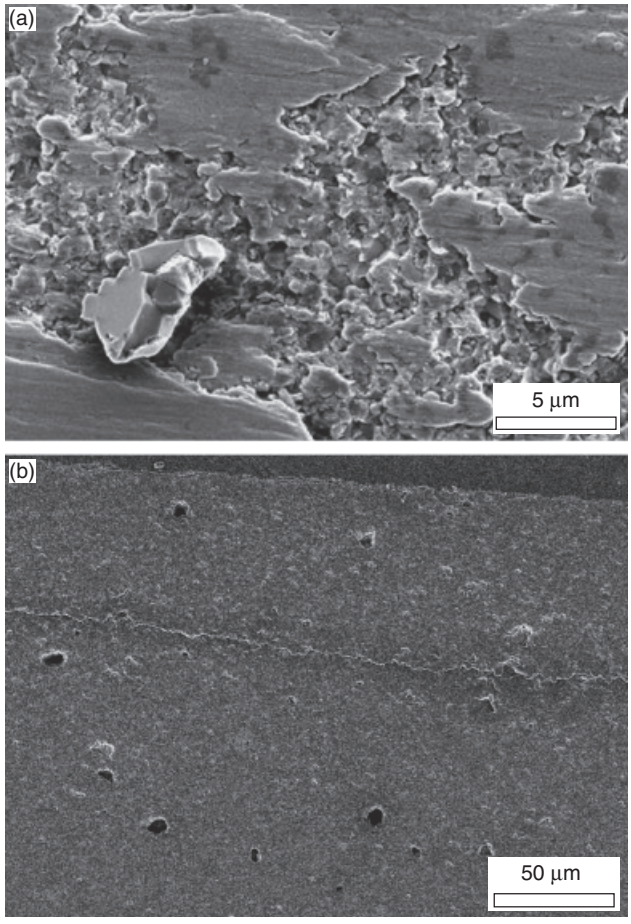

Fig. 11. Wear mechanisms in sintered material, which presented the lowest wear resistance. (a) Scanning electron micrograph of the worn surface. (b) Scanning electron micrograph of a cross section perpendicular to the worn surface.

with the Al_2O_3 matrix. This microstructure was obtained in directionally solidified Al_2O_3–$ZrO_2(Y_2O_3)$ oxides grown at low rates (10 mm/h) under conditions of coupled eutectic growth.[12] This microstructure was not achieved, however, in laser-melted surfaces because the compositional range for coupled eutectic growth in eutectic Al_2O_3–$ZrO_2(Y_2O_3)$ oxides is very narrow. Moreover, this eutectic shows a marked trend to undergo a transition on increasing the growth rate from the planar to the cellular growth regime and then to faceted cells.

It should be noted finally that the wear resistance of the sintered eutectic oxides was far lower than that of the laser-melted surfaces. Wear in the sintered material proceeded by the formation of large subsurface cracks, which ran parallel to the surface, and led to the pull-out of large fragments of the material (Fig. 11(b)). As a result, the worn surfaces were rougher (Fig. 11(b)) and the friction coefficient was higher (Fig. 7). Obviously, the lower porosity and higher hardness of laser-melted surfaces – which impeded the nucleation and growth of subsurface cracks – was the cause of the differences in wear resistance.

V. Conclusions

Fully dense, homogeneous, and crack-free Al_2O_3–$ZrO_2(Y_2O_3)$ eutectic oxide coatings were prepared by laser melting of the surface of sintered ceramic plates up to 7×50 mm^2. Laser power, traveling speeds, and preheating temperature of the ceramic substrate were selected to obtain thermal gradients at the solidification front of 700°C/mm equivalent to those found in rods grown by the laser-heated floating zone method. The sample surface was smooth, with an average roughness well below 1 μm and some occasional waviness associated mainly with laser instabilities. The microstructure of the layer was made up of colonies, elongated along the traveling direction, whose microstructural features (colony diameter, intercolony thickness, and interlamellar spacing) decreased as the traveling speed increased.

The Vickers hardness, friction coefficient, and specific wear resistance were measured at room temperature in a dry laboratory atmosphere. Hardness was at a maximum in the samples processed at a traveling speed of 500 mm/h, corresponding to a minimum in the friction coefficient and wear rate. This optimum behavior was correlated to the microstructural characteristics of the laser-melted material. Specimens grown at a lower traveling speed presented a coarser microstructure, while those grown at a higher speed revealed a higher population of defects (voids) at the intercolony regions. The wear rate of the optimum laser-melted specimens was almost an order of magnitude smaller than that of the conventionally sintered eutectic oxide material.

Acknowledgments

The authors thank Prof. V.M. Orera for useful discussions in the course of this work. F.J. Ester also wishes to acknowledge the help of the CSIC for the I3P contract co-financed by the European Social Fund and BSH Electrodomésticos.

References

[1]W. J. Minford, R. C. Bradt RC, and V. S. Stubican, "Crystallography and Microstructure of Directionally Solidified Oxide Eutectics," *J. Am. Ceram. Soc.*, **62**, 154–7 (1979).

[2]V. S. Stubican and R. C. Bradt, "Eutectic Solidification in Ceramic Systems," *Ann. Rev. Mater. Sci.*, **11**, 267–97 (1981).

[3]J. LLorca and V. M. Orera, "Directionally-Solidified Eutectic Ceramic Oxides," *Prog. Mater. Sci.*, **51**, 711–809 (2006).

[4]Y. Waku, N. Nakagawa, H. Ohtsubo, A. Mitani, and K. Shimizu, "Fracture and Deformation Behaviour of Melt Growth Composites at Very High Temperature," *J. Mater. Sci.*, **36**, 1585–94 (2001).

[5]J. LLorca, J. Y. Pastor, P. Poza, J. I. Peña, I. de Francisco, A. Larrea, and V. M. Orera, "Influence of the Y_2O_3 Content and Temperature on the Mechanical Properties of Melt-Grown Al_2O_3-ZrO_2 Eutectics," *J. Am. Ceram. Soc.*, **87** [4] 633–9 (2004).

[6]J. Y. Pastor, J. LLorca, A. Salazar, P. B. Oliete, I. de Francisco, and J. I. Peña, "Mechanical Properties of Melt-Grown Alumina-YAG Eutectics up to 1900K," *J. Am. Ceram. Soc.*, **88**, 1488–95 (2005).

[7]N. Bahlawane, T. Watanabe, Y. Waku, A. Mitani, and N. Nakagawa, "Effect of Moisture on the High-Temperature Stability of Unidirectionally Solidified Al_2O_3/YAG Eutectic Composites," *J. Am. Ceram. Soc.*, **83** [12] 3077–81 (2000).

[8]T. A. Parthasarathy, T.-I. Mah, and L. E. Matson, "Deformation Behavior of an $Al_2O_3/Y_3Al_5O_{12}$ Eutectic Composite in Comparison with Sapphire and YAG," *J. Am. Ceram. Soc.*, **76** [1] 29–32 (1993).

[9]J. Ramírez-Rico, A. R. Pinto-Gómez, J. Martínez-Fernández, A. R. de Arellano-López, P. B. Oliete, J. I. Peña, and V. M. Orera, "High-Temperature Plastic Behaviour of Al_2O_3–$Y_3Al_5O_{12}$ Directionally Solidified Eutectics," *Acta Mater.*, **54**, 3107–16 (2006).

[10]A. Sayir and S. C. Farmer, "The Effect of Microstructure on Mechanical Properties of Directionally Solidified Al_2O_3–$ZrO_2(Y_2O_3)$ Eutectic," *Acta Mater.*, **48**, 4691–7 (2000).

[11]J. A. Pardo, R. I. Merino, V. M. Orera, J. I. Peña, C. González, J. Y. Pastor, and J. LLorca, "Piezospectroscopic Study of Residual Stresses in Al_2O_3–ZrO_2 Eutectic Crystals," *J. Am. Ceram. Soc.*, **83**, 2745–52 (2000).

[12]J. Y. Pastor, J. LLorca, P. Poza, I. de Francisco, R. I. Merino, and J. I. Peña, "Mechanical Properties of Al_2O_3–$ZrO_2(Y_2O_3)$ Melt-Grown Eutectics with Different Microstructure," *J. Eur. Ceram. Soc.*, **25**, 1215–23 (2005).

[13]Y. Waku, S. Sakata, A. Mitani, K. Shimizu, and M. Hasebe, "Temperature Dependence of Flexural Strength and Microstructure of Al_2O_3–$Y_3Al_5O_{12}$–ZrO_2 Ternary Melt Growth Composites," *J. Mater. Sci.*, **37**, 2975–82 (2002).

[14]P. B. Oliete, J. I. Peña, A. Larrea, V. M. Orera, J. LLorca, J. Y. Pastor, A. Martín, and J. Segurado, "Ultra-High Strength Nanofibrillar Al_2O_3–YAG–YSZ Eutectics," *Adv. Mater.*, **19**, 2313–8 (2007).

[15]K. Miyoshi, S. C. Farmer, and A. Sayir, "Wear Properties of Two-Phase $Al_2O_3/ZrO_2(Y_2O_3)$ Ceramics at Temperatures from 296 to 1073 K," *Tribol. Int.*, **38**, 974–86 (2005).

[16]S. Bourban, N. Karapatis, H. Hofmann, and W. Kurz, "Solidification Microstructure of Laser Remelted Al_2O_3–ZrO_2 Eutectic," *Acta Mater.*, **45**, 5069–75 (1997).

[17]A. Larrea, G. F. de la Fuente, R. I. Merino, and V. M. Orera, "ZrO_2–Al_2O_3 Eutectic Plates Produced by Laser Zone Melting," *J. Eur. Ceram. Soc.*, **22**, 191–8 (2002).

[18]A. Larrea, V. M. Orera, R. I. Merino, and J. I. Peña, "Microstructure and Mechanical Properties of Al_2O_3–YSZ and Al_2O_3–YAG Directionally Solidified Eutectic Plates," *J. Eur. Ceram. Soc.*, **25**, 1419–29 (2005).

[19]D. Triantafyllidis, L. Li, and F. H. Stott, "Crack-Free Densification of Ceramics by Laser Surface Treatment," *Surf. Coat. Technol.*, **201**, 3163–73 (2006).

[20]F. J. Ester, R. I. Merino, V. M. Orera, A. Martín, J. Y. Pastor, and J. LLorca "Surface Modification by Laser Melting of Eutectic Ceramic Oxides"; pp. 297–304 Surface Modification Technologies XXI (21st International Conference on Surface Modification Technologies), Edited by T.S. Sudarshan and M. Jeandin. ASM International, OH, U.S.A.

[21]G. R. Anstis, P. Chantikul, B. R. Lawn, and D. B. Marshall, "A critical Evaluation of Indentation Techniques for Measuring Fracture Toughness: I, Direct Crack Measurements," *J. Am. Ceram. Soc.*, **64**, 533–8 (1981).

[22]A. Martín, M. A. Martínez, and J. LLorca, "Wear of SiC-Reinforced Al-Matrix Composites in the Temperature Range 20°C to 200°C," *Wear*, **193**, 169–79 (1996).

[23]J. Rodríguez, A. Martín, J. Y. Pastor, J. LLorca, J. F. Bartolomé, and J. S. Moya, "Sliding Wear of Alumina/Silicon Carbide Nanocomposites," *J. Am. Ceram. Soc.*, **82**, 2252–4 (1999).

[24]P. B. Oliete and J. I. Peña, "Study of the Gas Inclusions in $Al_2O_3/Y_3Al_5O_{12}$ and $Al_2O_3/Y_3Al_5O_{12}/ZrO_2$ Eutectic. Bers Grown by Laser Floating Zone," *J. Cryst. Growth*, **304**, 514–9 (2007).

[25]D. Triantafyllidis and L. Li, "Modelling of Boundary porosity Formation in Laser Melting and Resolidification of Ceramics," *J. Am. Ceram. Soc.*, **89**, 1286–94 (2006).

[26]R. I. Merino, J. I. Peña, V. M. Orera, A. Larrea, and A. J. Sánchez-Herencia, "Resolidificación Superficial de Eutécticos Al_2O_3-YSZ Asistida Por Láser," *Bol Soc. Esp. Ceram. V.*, **43**, 855–62 (2004).

[27]J. I. Peña, R. I. Merino, N. R. Harlan, A. Larrea, G. F. de la Fuente, and V. M. Orera, "Microstructure of Y_2O_3 Doped Al_2O_3–ZrO_2 Eutectics Grown by the Laser Floating Zone Method," *J. Eur. Ceram. Soc.*, **22**, 2595–602 (2002).

[28]J. H. Lee, A. Yoshikawa, H. Kaiden, K. Lebbou, T. Fukuda, D. H. Yoon, and Y. Waku, "Microstructure of Y_2O_3 Doped Al_2O_3/ZrO_2 Eutectic Fibers Grown by the Micro-Pulling-Down Method," *J. Cryst. Growth*, **231**, 179–85 (2001).

[29]J. F. Bartolomé, A. H. de Aza, A. Martin, J. Y. Pastor, J. LLorca, R. Torrecillas, and G. Bruno, "Alumina/Zirconia Micro/Nanocomposites, a New Material For Biomedical Applications with Superior Sliding Wear Resistance," *J. Am. Ceram. Soc.*, **90**, 3177–84 (2007).

[30]J. F. Bartolomé, C. Pecharromán, J. S. Moya, A. Martín, J. Y. Pastor, and J. LLorca, "Percolative Mechanism of Sliding Wear of Alumina/Zirconia Composites," *J. Eur. Ceram. Soc.*, **26**, 2619–25 (2006). □